MITSUBISHI ELECTRIC

MITSUBISHI ELECTRIC R&D CENTRE EUROPE

High Frequency Modelling of Permanent Magnet Synchronous Machine

Nicolas Voyer

Guilherme Bueno-Mariani

Abdelhadi Besri

Vincent Quemener

Yuriko Okamoto

Akire Satake

High Frequency Modelling of Permanent Magnet Synchronous Machine

Nicolas Voyer
Power Electronic Systems
Mitsubishi Electric R&D Center Europe
Rennes, France
n.voyer@fr.merce.mee.com

Guilherme Bueno Mariani
Power Electronic Systems
Mitsubishi Electric R&D Center Europe
Rennes, France
g.buenomariani@fr.merce.mee.com

Abdlehadi Besri
Mitsubishi Electric R&D Center Europe
Mitsubishi Electric R&D Center Europe
Rennes, France
a.besri@ fr.merce.mee.com

Vincent Quemener
ELSYS Design
Rennes, France
v.quemener@fr.merce.mee.com

Yuriko Okamoto
Advanced Technology R&D Center
Mitsubishi Electric
Amagasaki, Japan
okamoto.yuriko@ay.mitsubishielectric.co.cp

Akira Satake
Advanced Technology R&D Center
Mitsubishi Electric
Amagasaki, Japan
satake.akira@dy.mitsubishielectric.co.cp

Abstract—**This paper addresses the modelling of PMSM under high frequency PWM control. The high frequency components of input voltage have different responses in terms of induced current and iron losses, due to eddy currents in the magnets, phase conductors and in the core lamination. Both inductance and HF iron loss behavior of the machine were investigated through experiment, modelled, and reproduced by circuit simulation. Inductance is treated separately for low frequency and high frequency components to build the current response of the machine. HF iron losses are determined for each HF cycle individually, according to peak-to-peak HF current. The configuration of the model can be realized either from locked rotation tests or from Finite Element Analysis. The model is suited for the optimization of control strategy with respect to losses, including adaptation of switching frequency or over-modulation.**

Keywords—PMSM, modelling, iron losses, screening

I. Introduction

Permanent Magnet Synchronous Machines (PMSM) are largely used in industry for its high efficiency and high torque density. For such machines, the overall losses are generally quite low, and losses resulting from HF components are proportionally higher than for other machines. The thermal dimensioning of PMSM is typically realized through Finite Element Analysis tools, incorporating physical and heuristic loss models, and typical PWM current waveforms under nominal operation conditions.

In practice, machines are operated over large operation regions, and it is generally desirable to adapt the control of the inverter feeding the machine according to the desired mission profile (e.g. speed/torque profile, minimized losses, minimized torque ripple, …). This results in current waveforms that are typically quite different from the ones used at the time of PMSM dimensioning. It is therefore desirable to finely model the response of PMSM, in terms of current induction and losses, to any HF control strategies.

The motivation of the present paper is to build a circuit equivalent model of the machine able to predict the total losses with a good accuracy for any HF control pattern. Our study focused on 1.1kW PMSM used in commercial HVAC application.

A first key issue, explored in section II, is to reproduce the current waveform from PWM voltage patterns applied by motor inverter. HF inductance was measured showing impacts of saturation, cross saturation and screening. A phenomenological model is proposed able to reproduce HF current with good accuracy.

Section III presents a methodology for evaluating and characterizing HF iron loss from measured (or modelled) motor currents and voltage waveforms. A heuristic model is proposed and compared with measurement.

Section IV investigates the implementation of both inductance and HF iron loss models in circuit-simulation platform (PSIM).

II. HF Inductance Measurement

A. Measurement methodology

Long-term inductance relates the induced flux to the current. The differential (short-term) inductance in contrast relates the variations of induced flux with the variations of current. For currents applied in d-axis or in q-axis, both inductances take different values, due to the saliency of the machine. For each axis, the long-term and short inductances also differ mainly due to the saturation of the machine.

$$L_{ST} = \frac{d\phi}{dI} = \frac{d(L_{LT}I)}{dI} = L_{LT} + I\frac{d(L_{LT})}{dI} \tag{1}$$

Short-term inductance also varies with the frequency of the current waveform, due to screening effects resulting from eddy currents in conducting materials. As a result, the short-term inductance is different for the fundamental/rotational frequency and for PWM harmonics.

Through analysis of successive peak-to-peak levels $\Delta I_k, \Delta\phi_k$ of current and of induced flux, the estimation of inductance can be obtained through Minimum Mean Square Error (MMSE) analysis.

$$\Omega(L) = \sum(\Delta\phi_k - L\Delta I_k)^2 \tag{2}$$

$$\widehat{L_{ST}} = L|\Omega(L) = \min_{\forall L}(\Omega(L)) \tag{3}$$

MMSE estimation of inductance is then given by :

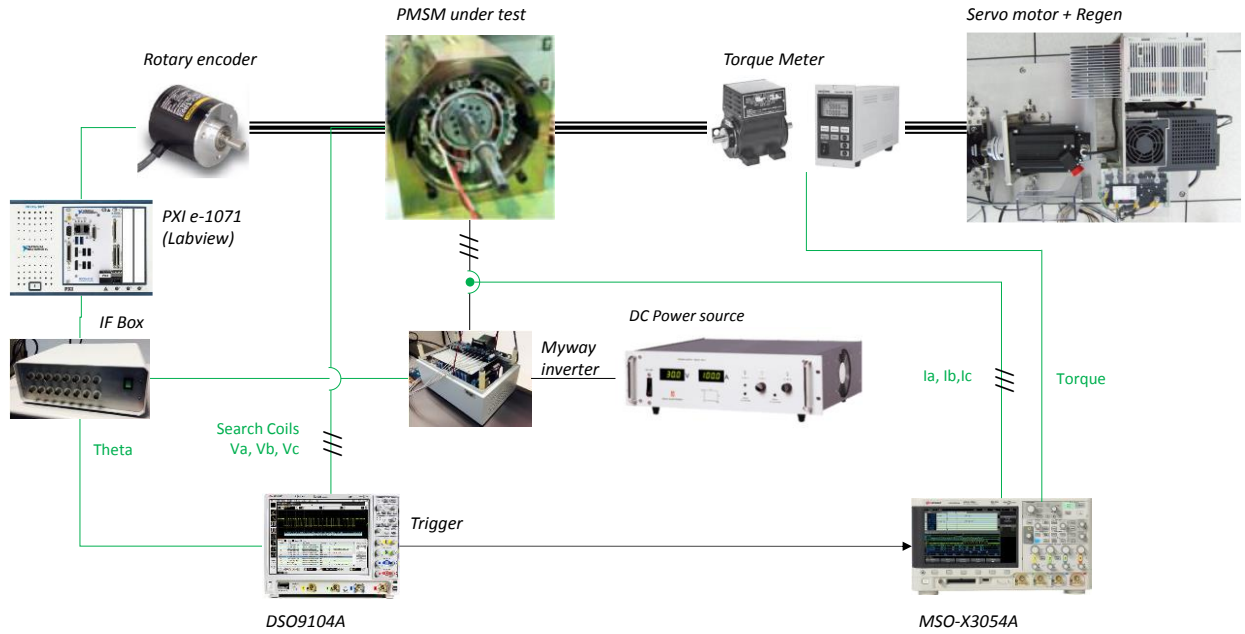$$\widehat{L_{ST}} = \frac{\sum\Delta\phi_k\Delta I_k}{\sum\Delta I_k^2} \tag{4}$$

Fig. 1. Experimental setup used for PMSM rotational tests

B. Measurement testbench

Fig. 1 shows the experimental system used for the estimation of inductance. Measurement were realized through rotational tests, over an exploration space defined by different rotational speeds, switching frequencies, and currents levels, in both d and q axis.

The test bench was driven by a LabVIEW controller, applying field oriented vector control, fed with position information from rotary encoder.

To feed equation (4) with proper estimations of induced flux, we equipped our experimental system with search coils on each tooth of the machine.

Voltage and current waveforms were simultaneously acquired on three phases using two synchronised high-frequency, high-storage oscilloscopes. For wide range of operation points (speed, currents, switching frequency), Data were collected over typically two million consecutive samples for offline analysis, according to (4).

The flux ϕ_{abc} induced by the current is estimated from search coil voltage (to get rid of Ohmic voltage drops along conductors, which vary with temperature and frequency) with and without current (representing the BEMF induced by permanent magnets). This induced voltage is simply

multiplied by the number of turns around each tooth according to (5) :

$$\phi_{abc} = \int N_t \big(V_{abc}(t) - V_{abc}(\theta(t), I_{abc} = 0)\big)\, dt \qquad (5)$$

To get rid of uncertainty of initial flux values in (5), recalibration was realized to ensure zero average flux over few consecutive fundamental periods. Voltage waveforms with and without current are post-synchronized using the rotor angle information obtained by the rotary encoder.

We estimated distinct short-term inductance for fundamental and switching frequencies, using a separation of high and low frequency terms of measured current and flux. HF/LF separation is realized iteratively, using successive Low-Pass Filtering (LPF) of waveforms so as to properly split the two components while keeping integrity of total waveform. LPF frequency is chosen as to reject the HF component and keep the LF component. Using the proposed process, typical voltage and current waveforms can be decomposed in its HF and LF components, as shown in Fig 2.

The accurate detection of peak-to-peak HF current is made difficult due to current ringing oscillations caused by the switching events of inverter. Specific processing was made to skip current measurement samples right before switching events. As seen on Fig. 3, only current samples
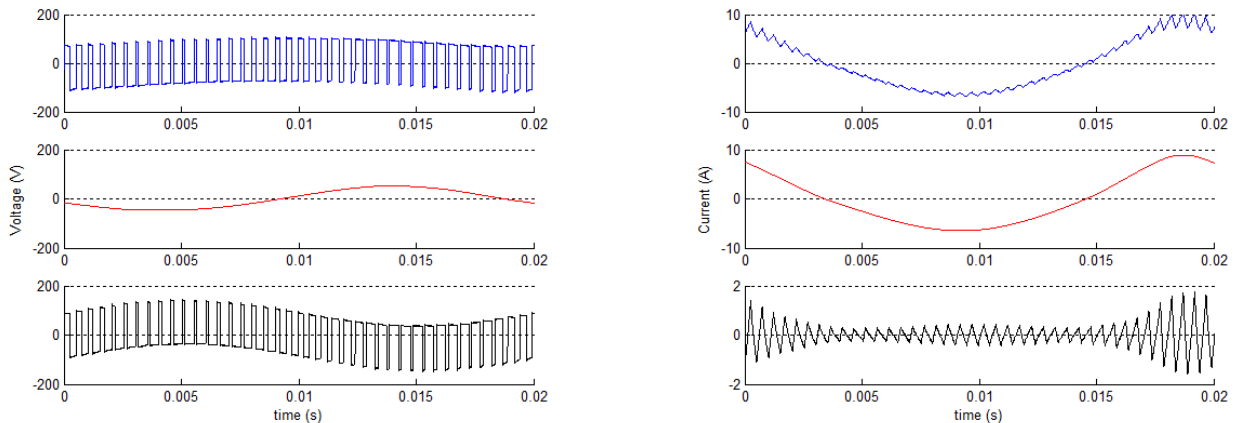

Fig. 2. HF/LF decomposition of typical PWM (left) Voltage and (right) Current waveforms (blue) input ; (red) low frequency ; (black) High-frequency
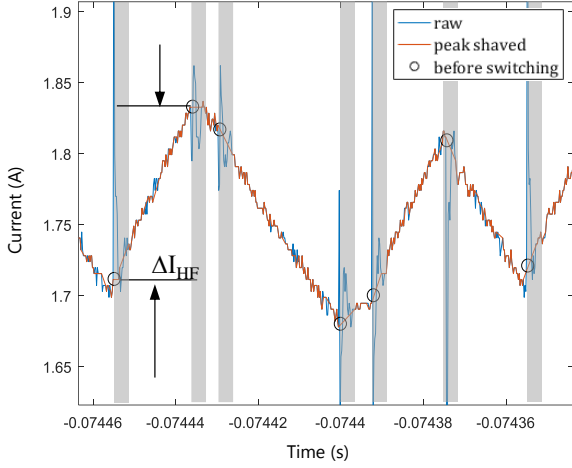
Fig. 3. Detailed view of current waveform around switching events

measured just before the switching (circles) are needed to compute a peak-to-peak current level between switching events.

Failing to consider ringing events causes an overestimation of peak-to-peak current, which in turn would lead to underestimation of HF inductances.

C. LF long-term Inductance measurement

Long-term inductance results are gathered in Fig. 4. It can be observed that saturation of L_d is not even, due to magnetic field imposed by permanent magnets. Demagnetization fields ($I_d < 0$) hardly impact the L_d inductance while magnetization fields ($I_d > 0$) quickly drives the machine towards saturation. Reversely, the saturation of L_q inductance due to current in q-axis is symmetric.

D. HF short-term Inductance measurement

Fig. 5 collects measurement results for different switching frequencies and current levels. Compared with the long-term inductances of Fig. 4, the high-frequency short-term inductances, also prone to saturation with the current, take significantly lower levels. Due to relation (1), the effect of saturation is indeed amplified. We also observe that cross-saturation is less pronounced than saturation.

Fig. 5 mainly shows that HF inductances are strongly affected by frequency screening. When switching frequency gets high, the fast variations of flux hardly flow through the heart of magnetic materials, which offer less penetration in
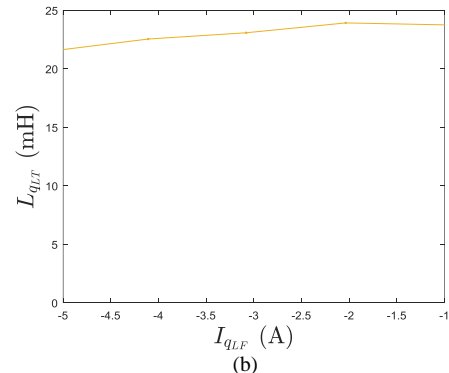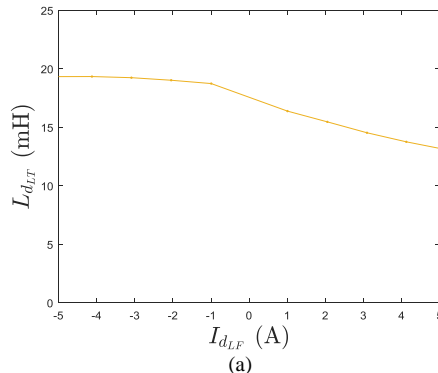
presence of eddy currents (skin effect). This causes the differential inductance to drop, by up to 30% between 2 and 20 KHz, comparable to the drop of inductance resulting from saturation due to high magnetizing current.

The screening drop in inductance is noticeably reduced in presence of saturation (as magnetic materials already exhibit less permeability).

The drop ratio between LF and HF inductances can reach up to 40%. Thermal design of motor using current waveform generated with LF inductance only, would typically lead to underestimated HF current swings, and underestimated HF iron losses.

Fig. 6 shows the saturation of the machine for various rotational speeds, and a switching frequency of 2KHz. Surprisingly, HF inductances seem to also varies with the rotational speed. Indeed, HF components in dq axis frame (as seen from the rotor) are projected on the abc frame (i.e. stator side) as a difference between HF+LF and HF-LF terms, causing interactions between HF and LF terms. In contrast to switching frequency, increasing rotational speeds tend to increase the HF inductances. In other words, rotational speed reduces the level of screening.

E. HF Inductance Model

Impact of saturation can be modelled considering a typical saturation law expressed as

$$\phi = \frac{2}{\pi}\phi_{max}atan(\alpha I) \tag{6}$$

Then using (1), the differential inductance would vary with current according to (7).

$$L_{ST} = \frac{2\alpha\phi_{max}}{\pi}\frac{1}{1+\alpha^2 I^2} \tag{7}$$

Considering (7), we therefore proposed and investigated a phenomenological model able to reproduce the observations made in Figs. 5 to 6. This model is summarized in (8).

$$L_{HF} = k_1 + \frac{k_2}{1+k_3(I_d+k_4)^2}\frac{1}{1+k_5 I_q{}^2}\frac{1}{1+k_6 f_{sw}+k_7 f_{sw}{}^2}\frac{1}{1+k_8/f_{AC}+k_9/f_{AC}{}^2} \tag{8}$$

In d axis, the magnetic material also experiences the remanent flux from the permanent magnet, so that equation (7) needs to be shifted correspondingly with parameter k_4.
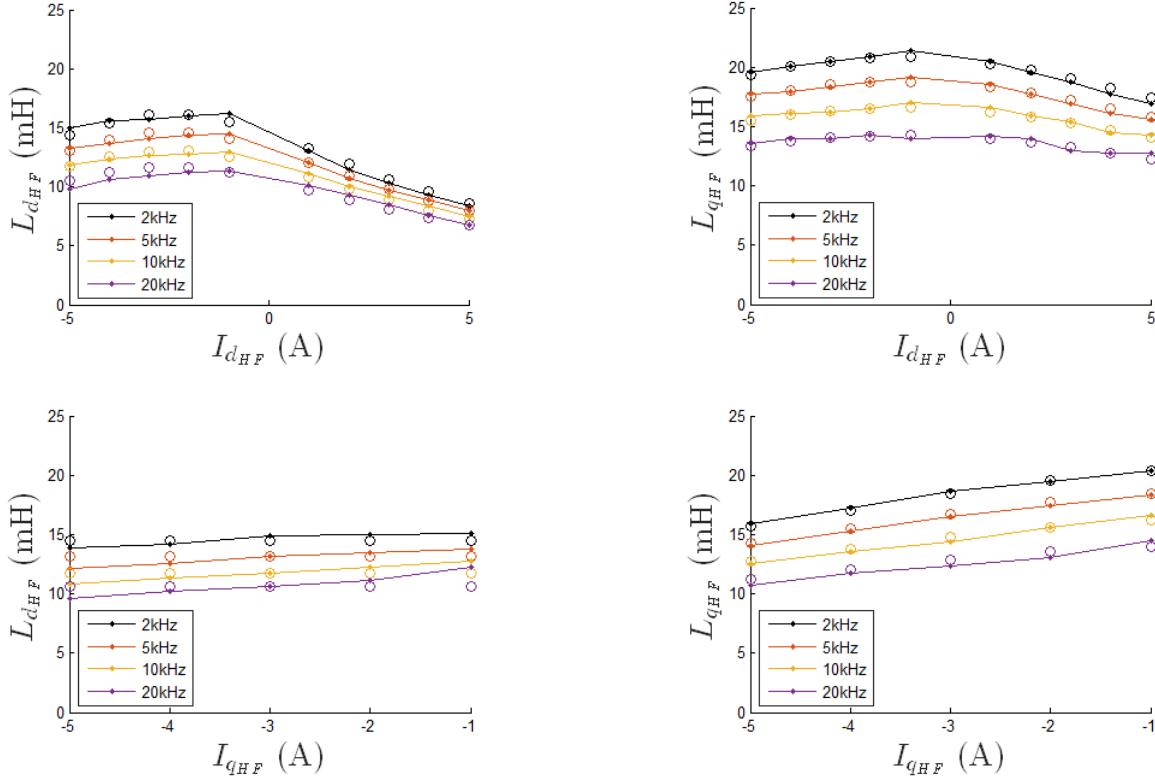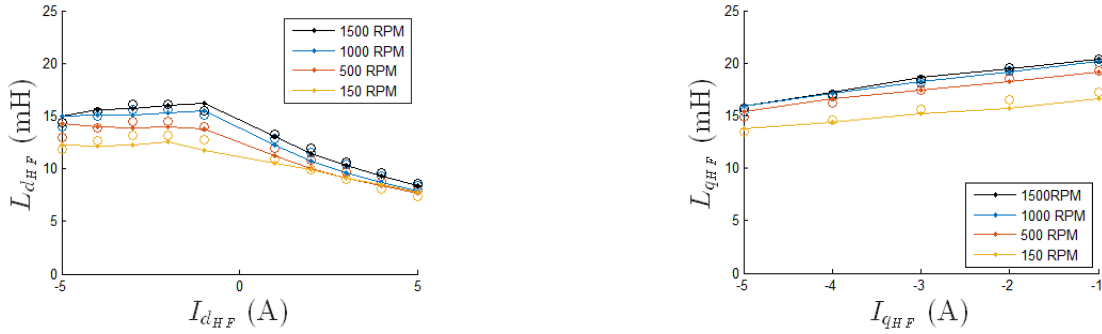

Fig. 4. Variations of low frequency long-term inductance with current in (a) d-axis or (b) in q axis

Fig. 5. Impact of switching frequency on short-term High frequency inductance. (left) : L_d (right) : L_q (top) : variation with I_d, (down) : variation with I_q ; (lines) : Measurement (circles) : proposed Model

Parameters $\{k_1 \dots k_9\}$ of proposed inductance model take different values for d and q axis. We automated the extraction of these parameters from measurement data using least-square minimization routine.

The parameter extraction produces a model which nicely reproduces measured variations of inductances, as seen in Fig. 5 and 6. The model is effective in reproducing, both qualitatively and quantitatively, the experimentally-observed phenomena, such as saliency, saturation, cross-saturation, screening, screening reduction under high speeds.

III. HF IRON LOSS MODELLING

A. Measurement methodology

Our interest was put in modelling HF iron losses, resulting from hysteresis, eddy current and excess losses. Depending on operating conditions, such losses may be small compared with total other losses of the machines (LF iron losses, LF+HF copper losses).

A simple way to estimate HF iron losses with good accuracy, consists in using the HF current and search coil voltage waveforms that no longer contains any low frequency components, nor the voltage drops representative of copper losses.

$$P_{HF} = P_{HF_d} + P_{HF_q} = E\left(V_{HF_d} I_{HF_d}\right) + E\left(V_{HF_q} I_{HF_q}\right) \quad (9)$$

To avoid bias in (9), it is crucial that LF/HF separation of input waveforms is effective, without residual cross talk between LF and HF terms.

B. HF iron loss measurement

The results obtained experimentally with (9) are gathered in Fig. 7 and 8. They clearly indicate that HF iron losses increase with saturation, rotational speed, and reduce with switching frequency. This advocates for possibility of optimization of control, as the increase of switching losses can potentially be recovered by a reduced level of HF iron losses.
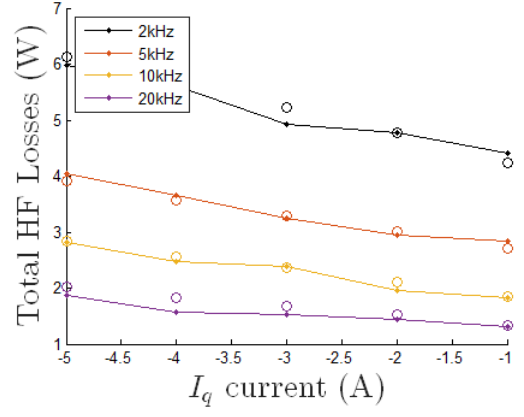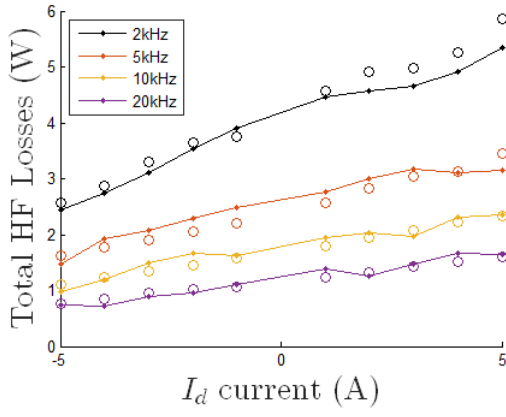
Fig. 7. Impact of switching frequency on HF iron losses (lines) : Measurement (circles) : Model
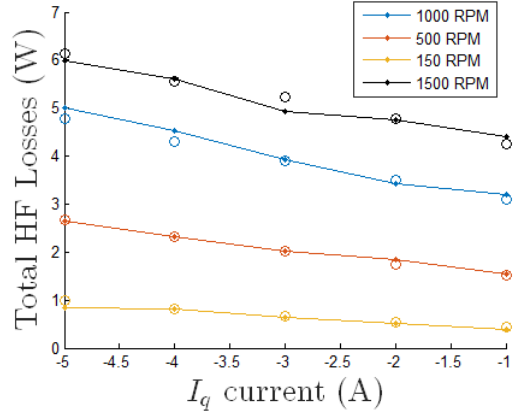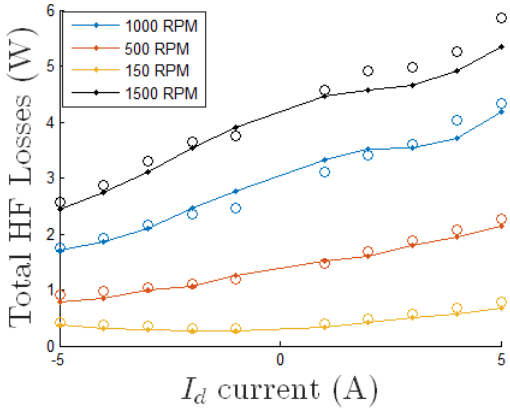

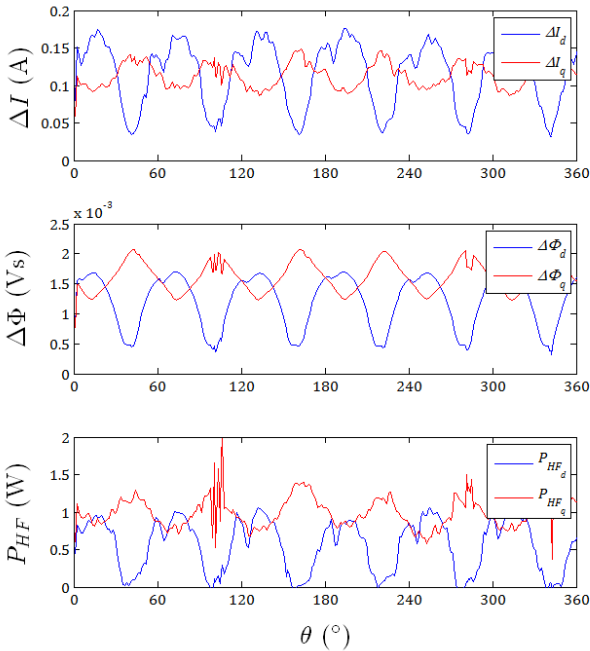Fig. 8. Impact of rotational speed on HF iron losses (lines) : Measurement (circles) : Model

Fig. 9. Evolution of peak-to-peak HF current, HF flux, HF losses with rotor angle

Fig. 9 shows the time evolution of the peak-to-peak of flux and of current for a given operation point (1500 rpm, 20 KHz, -3A in q axis). It shows that the HF iron losses in both d and q axis have clear distinct patterns, and that time variations of HF iron losses of each axis (computed from (9) between consecutive switching events) seem to better follow the variations of the current rather than that of induced flux.

C. Phenomenological Model

While Bertotti formula, that takes peak-to-peak flux as input for iron losses, is widely spread in the community, our observation on dependency of HF losses with peak-to-peak current led us consider another model, using both peak-to-peak current and flux terms.

Further considering that rising and descending times vary along test, and considering that switching frequency is not a good indicator of HF losses under over-modulation, we modified the model to take the duration between consecutive switching events in place of switching frequency. The proposed model for iron energy losses is thus expressed for each kth switching subcycle as

$$E_{HF_k} = \alpha \Delta t_k{}^{\alpha_t} \Delta I_k{}^{\alpha_I} \Delta \phi_k{}^{\alpha_\phi} \tag{10}$$

Subcycles Δt_k are time intervals between consecutive peaks of HF induced flux and current, corresponding to switching events. Consecutive peaks typically take different timings in d and in q axis.

The procedure for extraction of parameters $\{\alpha, \alpha_t, \alpha_I, \alpha_\phi\}$ is similar to that of parameters of inductance model. We searched for coefficients able to reproduce

individually measured HF loss per cycles in both d and q axis. To that end, we used a minimum mean square criterion of a strong relationship expressed by (11).

$$\min_{(\alpha,\alpha_t,\alpha_I,\alpha_\phi)} \left(\sum_k \left(\Delta t_k P_{HF_k} - \alpha \Delta t^{\alpha_t} \Delta I^{\alpha_I} \Delta \phi^{\alpha_\phi} \right)^2 \right) \quad (11)$$

Parameters $\{\alpha, \alpha_t, \alpha_I, \alpha_\phi\}$ take different values in d and q axis, and are shown in table I.

TABLE I – EXTRACTED PARAMETERS OF HF LOSS ROTATIONAL MODEL

Parameter	D axis	Q axis
α	0.42	0.0032
α_t	-0.0093	-0.0076
α_I	0	1.082
α_ϕ	1.686	0.44

The result of modelling are compared with measured loss levels in Figs. 7 and 8, showing a remarkable fit.

D.   Verification under overmodulation conditions

We verified the validity of the iron loss model under different control strategy. We reduced the level of DC bus feeding the motor inverter, so that each leg regularly experiences over-modulation. In over-modulation conditions, the frequency carrier gets below the modulation wave, and PWM operation of inverter leg stops until the modulation wave goes below the DC bus voltage. As a result, the duration of subcycles are affected. At phase level, a subcycle could last as long as the half of the fundamental cycle. In practice, only one phase gets over-modulated at a time, so that the number of subcycles per switching cycle varies from 4 to 6. We applied the HF loss model developed from normal rotational tests on over-modulated test data. The results are gathered in Fig. 10. The proposed model can reproduce HF iron loss with a fair level of accuracy (below 20%).

IV.   CONCLUSIONS

In this paper we have developed a high-frequency model of PMSM, able to reproduce current waveform under HF screening, and HF iron losses under over-modulation conditions. The proposed model can be configured using rotational test data. The model brings benefits in the optimisation of motor drive control and could be used in circuit simulation for comparing various control strategies.

To build this model, we also developed analysis methodology to assess the HF inductance of the machines, and the HF iron loss per switching subcycle. Results show the importance of modelling frequency screening due to presence of eddy currents in conductive materials.

REFERENCES

[1]   A. Krings, J. Soulard and O. Wallmark, "Influence of PWM switching frequency and modulation index on the iron losses and performance of slot-less permanent magnet motors," *2013 International Conference on Electrical Machines and Systems (ICEMS)*, Busan, 2013, pp. 474-479

[2]   K. Yamazaki, T. Fukuoka, K. Akatsu, N. Nakao and A. Ruderman, "Investigation of Locked Rotor Test for Estimation of Magnet PWM Carrier Eddy Current Loss in Synchronous Machines," in *IEEE Transactions on Magnetics*, vol. 48, no. 11, pp. 3327-3330, Nov. 2012.
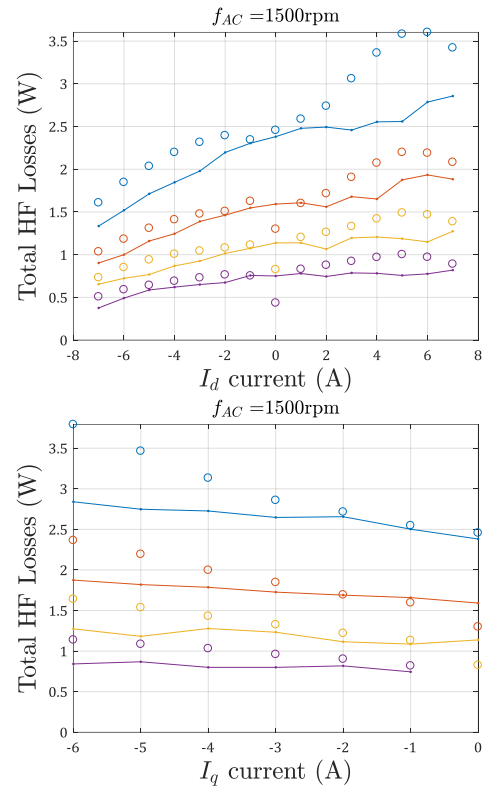
Fig. 10. Total HF iron losses in over-modulation conditions ; (lines) Measurement (circles) Model

[3]   K. Akatsu, K. Narita, Y. Sakashita and T. Yamada, "Impact of flux weakening current to the iron loss in an IPMSM including PWM carrier effect," *2009 IEEE Energy Conversion Congress and Exposition*, San Jose, CA, 2009, pp. 1927-1932.

[4]   M.S. Muhit and R. Hoque, "Magnetic and Electric Characterization of Materials for Electrical Machines", *International Journal of Scientific & Engineering Research*, vol. 4, no. 8, pp785-791, August 2013

[5]   D. Lee, Y.-J. Kim and S.-Y. Jung, "Numerical Analysis on Iron Loss and PM Loss of PMSM Considering Carrier harmonics", *Journal of Magnetism*, 18(2), 216-219 (2013)

[6]   B. Gaussens, E. Hoang and O. de la Barrière, "Uni- and Bidirectional Flux Variation Loci Method for Analytical Prediction of Iron Losses in Doubly-Salient Field-Excited Switched-Flux Machines," in *IEEE Transactions on Magnetics*, vol. 49, no. 7, pp. 4100-4103, July 2013.

[7]   W. Hassan and B. Wang, "Efficiency optimization of PMSM based drive system," *Proceedings of The 7th International Power Electronics and Motion Control Conference*, Harbin, 2012, pp. 1027-1033.

[8]   K.-J. Lee, H. Cha, J.P. Lee, D.-W. Yoo and H.-J. Kim "Experimental and Numerical Analysis of a Simple Core Loss Calculation for AC Filter Inductor in PWM DC-AC Inverters". *Journal of Power Electronics* (2013)

[9]   H. Matsumori, T. Shimizu, K. Takano and H. Ishii, "Comparison between single phase and three phase of PWM inverters in Iron Loss measurement," *2012 15th International Power Electronics and Motion Control Conference (EPE/PEMC)*, Novi Sad, 2012, pp. DS1d.3-1-DS1d.3-8.

[10]   C. R. Sullivan, J. H. Harris and E. Herbert, "Core loss predictions for general PWM waveforms from a simplified set of measured data," *2010 Twenty-Fifth Annual IEEE Applied Power Electronics Conference and Exposition (APEC)*, Palm Springs, CA, 2010, pp. 1048-1055.

[11]   C. R. Sullivan, "Overview of core loss prediction (and measurement) techniques) for non-sinusoidal waveforms" *APEC 2012*

[12]   J. Muhlethaler, J. Biela, J. W. Kolar and A. Ecklebe, "Improved Core-Loss Calculation for Magnetic Components Employed in Power Electronic Systems," in *IEEE Transactions on Power Electronics*, vol. 27, no. 2, pp. 964-973, Feb. 2012.